Rotational Test of Flexible Rotor Supported by Active Magnetic Bearings (Passing the 3rd Bending Critical Speed)

Makoto Ito

Dept. of Development

Shinkawa Sensor Technology Inc.

4-22 Yoshikawa-kogyodanchi, Higashihiroshima-shi, Hiroshima, Japan

itom@sst.shinkawa.co.jp

Hiroyuki Fujiwara and Osami Matsushita

Dept. of Mechanical Engineering

National Defense Academy

1-10-20 Hashirimizu, Yokosuka-shi, Kanagawa, Japan

hiroyuki@nda.ac.jp, osami@nda.ac.jp

***Abstract* – In industrial rotational machinery, it has been required that a long span and a high-speed rotor are designed in order to improve efficiency and reduce costs. In concerning many flexible rotors, the 1st bending critical speed and the 2nd bending critical speed have been passed, but never the 3rd critical speed. In this study a flexible rotor having the 3rd bending critical speed within the rated speed was designed, and was tested to pass the 3rd bending critical speed, owing to fine tuning of Active Magnetic Bearing controller and accurate balancing method.**

***Index Terms* – Active Magnetic Bearing, Mode Separation Control, Sensitivity Function, Q-value, 3rd Bending Critical Speed**

1. INTRODUCTION

An industrial rotating machine supported by active magnetic bearings (AMBs) requires a lighter rotor turning at a higher speed. For example, for a centrifugal compressor, a type of industrial rotating machine, not only can its mechanical performance be improved by making the rotor fast, long, and light, but its manufacturing cost can also be reduced [1]. Accordingly, the industry is now hoping for a major advance in mechanical performance and a substantial reduction in the manufacturing costs by making faster, longer, and lighter rotors. To satisfy these requirements, it is essential to establish the technology for an AMB-supported flexible rotor to pass its high order bending critical speed that corresponds to the 2nd bending mode or higher. However, although there have been a few reports concerning rotors corresponding to the 2nd bending mode [2,3], there are no reports concerning rotors corresponding to the 3rd bending mode.

We have worked on the technology for an ABM-supported symmetrical and flexible rotor passing its critical speed that corresponds to the 3rd bending mode. This paper describes (1) how to design a control system based on mode separation control and a controller based on a phase shift [4], (2) the results of an evaluation of the stability margin of the control system according to the sensitivity function standardized according to ISO 14839-3 [5], (3) the results of an evaluation of the damping performance of the control system by measuring the Q-value (response magnification) using the Q-value function and the half power point [6], and (4) the results of a test in which the rotor passes the critical speed corresponding to the 3rd bending mode in the mode-by-mode balancing method [3].

2. EXPERIMENTAL SYSTEM

2-1. Structure of Experimental System

Figure 1 shows the structure of the experimental system. Radial AMBs are placed at the both side, a thrust AMB at the far left, and a non-contact flat motor at the far right. Furthermore, placing the AMB and other components in a vacuum chamber enables operation in vacuum.

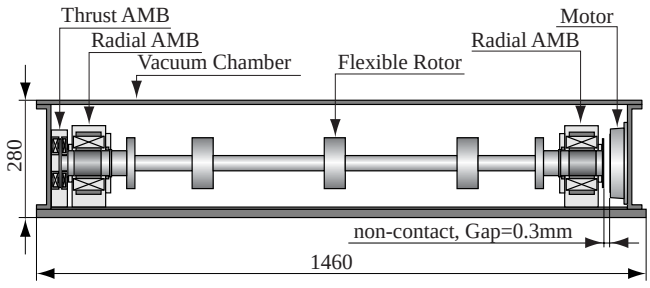

Fig. 1 Structure of experimental system

2-2. Modeling

Figure 2 (upper part) shows the structure of a flexible rotor. The length is 1,310 mm, the mass is 31.4 kg, and the shaft diameter is 37 mm. The rotor is symmetrical in longitudinal direction, and the purpose of the five disks of the rotor in the figure is to attach correction weights.

The equation of motion of the rotor AMB, ignoring the

damping term, is as follows:

$$\mathbf{M}\begin{bmatrix}\ddot{\mathbf{X}}_1\\ \ddot{\mathbf{X}}_2\end{bmatrix}+\mathbf{K}\begin{bmatrix}\mathbf{X}_1\\ \mathbf{X}_2\end{bmatrix}=\begin{bmatrix}\mathbf{Q}_{\mathrm{AMB}}\\ \mathbf{0}\end{bmatrix} \tag{1}$$

where $\mathbf{X}_1$ is the AMB boundary displacement at the both side, $\mathbf{X}_2$ is the inner mode displacement other than the AMB boundary displacement, $\mathbf{M}$ is the mass matrix, $\mathbf{K}$ is the stiffness matrix, $\mathbf{Q}_{\mathrm{AMB}}$ is the control force which is generated by the AMB according to the $\mathbf{X}_1$. Coordinate conversion of equation (1) using the mode conversion matrix Φ provides the equation of motion after applying the mode synthesis method as shown in equation (2), and this Finite Element Method (FEM) model is reduced to the seven degrees of freedom (7DOF) model by using the component mode synthesis method [4].

$$\mathbf{M}_\Phi\begin{bmatrix}\ddot{\mathbf{X}}_1\\ \ddot{\boldsymbol{\eta}}\end{bmatrix}+\mathbf{K}_\Phi\begin{bmatrix}\mathbf{X}_1\\ \boldsymbol{\eta}\end{bmatrix}=\begin{bmatrix}\mathbf{Q}_{\mathrm{AMB}}\\ \mathbf{0}\end{bmatrix} \tag{2}$$

where $\mathbf{M}_\Phi=\Phi^t\mathbf{M}\Phi$ is modal mass matrix of mode synthesis method, $\mathbf{K}_\Phi=\Phi^t\mathbf{K}\Phi$ is modal stiffness matrix of mode synthesis method.

In this study, we used the mode synthesis method to create a 7 DOF model and analyzed up to the fifth bending mode, expected to be the spill-over point. Figure 2 (lower part) shows the vibration modes of the rotor when a free-free condition is given. Since the AMBs are supported flexibly, the rotor should have vibration modes as indicated in Figure 2 at each critical speed. The rotor is found to be a flexible rotor with the third bending critical speeds $\mathrm{N_{C5}}$ up to the rated speed of 300 rps. $\mathrm{N_{C1}}$, $\mathrm{N_{C2}}$ are the rigid mode's critical speeds, and $\mathrm{N_{C3}}$, $\mathrm{N_{C4}}$, $\mathrm{N_{C5}}$ are the bending mode's critical speeds.

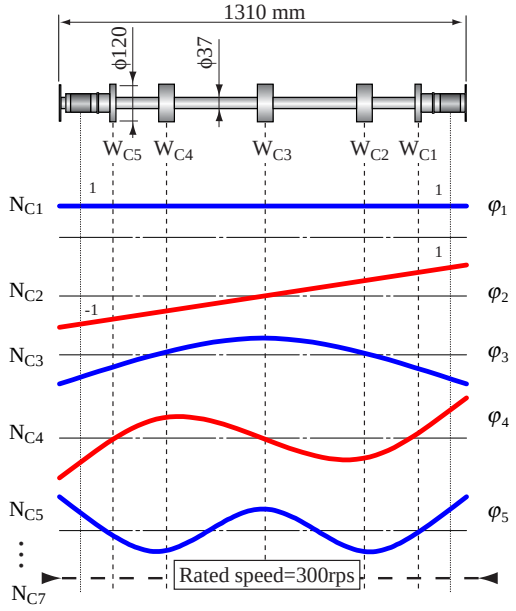

Fig. 2 Mode of the rotor (free-free condition)

3. CONTROL SYSTEM

3-1. Controller Configuration

In this study, we designed a control system based on mode separation control method [4]. This control method allows us to design individual controllers for each separated system and widens the bandwidth between adjacent natural frequencies, which also makes it easy to insert a variety of filters into the controllers.

Figure 3 shows a block diagram of our control system. A divider separates the signals x_1 and x_2 derived from displacement sensors arranged close to the left and right radial AMBs into the displacement x_p of the translating mode and the displacement x_t of the tilting mode. These separated signals are changed to the mode control signals v_p and v_t via the controllers G_{rp} and G_{rt}. After this, the control signals v_1 and v_2 are regenerated for the left and right AMBs and a power amplifier (PWM) drives them according to the control signals.

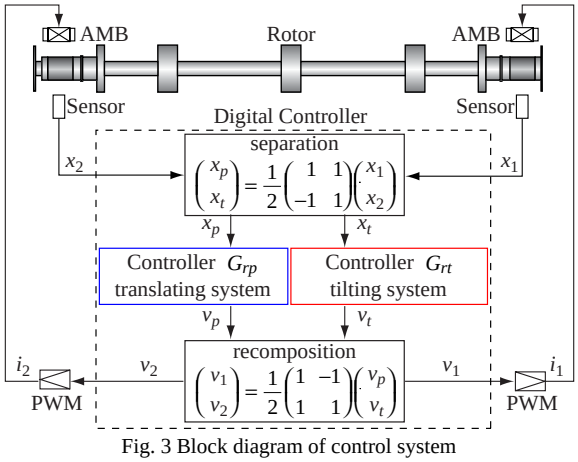

Fig. 3 Block diagram of control system

3-2. Controller Design

We designed a controller that consists of a main PID control circuit, a filter coping with instability caused by spill-over, and an phase shifter keeping the phase lead at the plant's natural frequency (positive damping) after the mode separation [4]. The transfer functions of the translating system controller G_{rp} and the tilting system controller G_{rt} designed are as follows:

$$G_{rp}=G_{\mathrm{PID1}}\times G_{\mathrm{PBF}}\times G_{\mathrm{NF}} \tag{3}$$

$$G_{rt}=G_{\mathrm{PID2}}\times G_{\mathrm{PSF}}\times G_{2\,\mathrm{LPF}} \tag{4}$$

where,

$$G_{\mathrm{PID1}}=24\times\left(\frac{1}{\tau_1 s+1}+\frac{\tau_2 s+1}{\alpha_1\tau_2 s+1}+\frac{\tau_3 s+1}{\alpha_2\tau_3 s+1}\right)$$

$$G_{\mathrm{PID2}}=48\times\left(\frac{1}{\tau_1 s+1}+\frac{\tau_4 s+1}{\alpha_3\tau_4 s+1}\right)$$

$$G_{\mathrm{PBF}}=\frac{1}{1-\alpha_4}\times\left(1-\frac{\alpha_4}{(\tau_5 s)^2+2\zeta_1(\tau_5 s)+1}\right)$$

$$G_{NF} = \frac{(\tau_6 s)^2 + 1}{(\tau_6 s)^2 + 2\zeta_1(\tau_6 s) + 1}$$

$$G_{PSF} = \frac{(\tau_8 s)^2 - 2\zeta_3(\tau_8 s) + 1}{(\tau_7 s)^2 + 2\zeta_2(\tau_7 s) + 1}$$

$$G_{2\,LPF} = \frac{1}{(\tau_9 s)^2 + 2\zeta_4(\tau_9 s) + 1}$$

G_{PID} is a PID control circuit, G_{PBF} is a Phase Bump Filter (PBF), G_{NF} is a Notch Filter (NF), and G_{PSF} is a Phase Shifting Filter (PSF), $G_{2\,LPF}$ is 2nd Low Pass Filter (2nd LPF). The other parameters are shown below:

$\tau_1 = 1/(2\pi \times 0.1)$, $\tau_2 = 1/(2\pi \times 25)$, $\tau_3 = 1/(2\pi \times 85)$, $\tau_4 = 1/(2\pi \times 35)$, $\tau_5 = 1/(2\pi \times 590)$, $\tau_6 = 1/(2\pi \times 665)$, $\tau_7 = 1/(2\pi \times 110)$, $\tau_8 = 1/(2\pi \times 135)$, $\tau_9 = 1/(2\pi \times 400)$, $\alpha_1 = 0.3$, $\alpha_2 = 0.1$, $\alpha_3 = 0.25$, $\alpha_4 = 0.63$, $\zeta_1 = 0.22$, $\zeta_2 = 0.11$, $\zeta_3 = 0.09$, $\zeta_4 = 0.2$

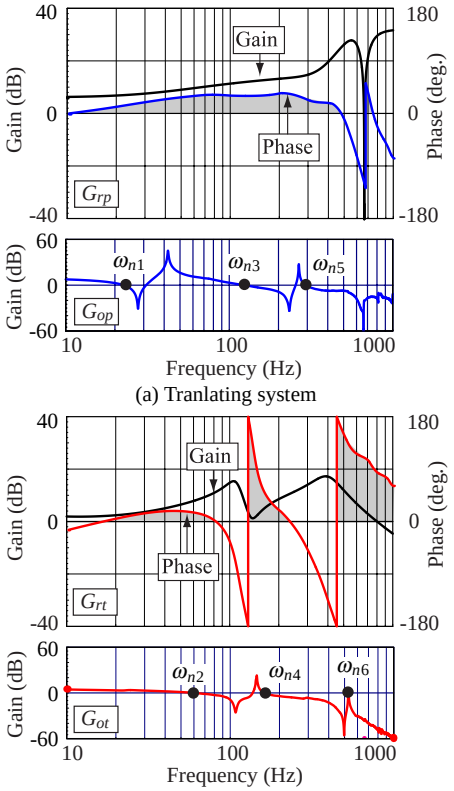

(a) Tranlating system

(b) Tilting system

Fig. 4 Bode plot of controller

Figure 4 shows the results of measuring the controller's transfer functions G_{rp} and G_{rt} in the translating and tilting systems as well as the gains $|G_{op}|$ and $|G_{ot}|$ of the open loop transfer functions. The gain crossover frequency of the open loop transfer function indicated by a black circle corresponds to the natural frequency of the closed loop transfer function. The shaded area shows the phase lead that the controller gives to the control system.

As shown in Figure 4(a), we designed the translating controller to keep the phase lead (positive damping) at the natural frequencies (ω_{ni} where $i = 1, 3, 5$) of the translating control system after the mode separation. We designed the tilting controller as well—at the natural frequencies (ω_{ni} where $i = 2, 4, 6$) of the tilting system as shown in Figure 4(b).

4. STABILITY MARGIN

With the sensitivity function, ISO FDIS 14839-3 defines criteria for evaluating the stability margin of the AMB supported flexible rotor used in this study [5]. The sensitivity function is represented by the following equation:

$$G_s = \frac{1}{1 + G_o} \tag{5}$$

where G_o is the open loop transfer function. Figure 5 indicates the measured sensitivity functions G_{sp} and G_{st} of the translating and tilting control systems. Figure 5(a) tells that the translating control system has a maximum sensitivity of 11 dB at ω_{n1} (Zone B specified in the ISO standards). Figure 5(b) says that the tilting control system has a peak sensitivity of 15 dB (Zone D) at ω_{n2}. According to ISO 14839-3 for safety operation, the tilting system must be reviewed to change the sensitivity at ω_{n2} from Zone D to Zone B or better. As a result, we measured the Q-value to evaluate the damping performance of the control system and to confirm whether or not to conduct a rotational test.

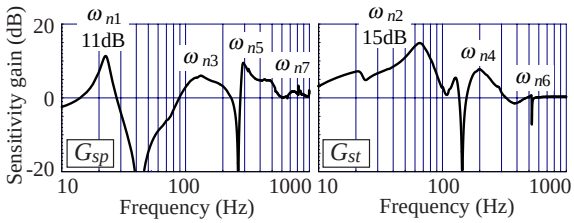

(a) Translating system (b) Tilting system

Fig. 5 Sensitivity function

5. Q-VALUE EVALUATION

5-1. Proposing of Q-value Function

ISO 10814 defines the criteria for evaluating the Q-value (resonance magnification) of a machine rotating at higher than its critical speed. The Q-value is represented by the following equation:

$$\text{Q-value} = \frac{1}{2\zeta\sqrt{1-2\zeta^2}} \approx \frac{1}{2\zeta} \tag{6}$$

where ζ is the damping ratio. Evaluating the Q-value is equivalent to estimating the damping performance of a control system at its resonance frequency.

In general, a rotor may be difficult to run at a high order bending critical speed since the Q-value is high and a sharp unbalance in the resonance appears. To turn a flexible rotor smoothly, it is necessary to measure the Q-value for prior evaluation. Accordingly, in this paper, we propose a new Q-value function that allows us to estimate the Q-value from the open loop transfer function of a rotor being suspended statically [6].

5-2. Theory of Q-value function

Figure 6 is a block diagram of an AMB-supported rotor system. The Q-value function can be derived from the sensitivity function when $H(s)$ is the transfer function of the flexible rotor except for the inertial term and the plant G_p^* is the inertial term given by altering Figure 6(a) to 6(b). The procedures for finding the Q-value function are described below.

- Step 1: Derive G_p^* from the measured G_p of only the flexible rotor. Note that the gain Γ and the phase Δ are estimated from the difference between the model's and measured plant transfer functions.

$$G_p^*(s) = \frac{G_p(s)}{\Gamma \times \Delta} \tag{7}$$

- Step 2: Derive $H(s)$ from G_p^*.

$$H(s) = \frac{1}{G_p(s)} - m^* s^2 \tag{8}$$

Note that the modal mass m^* can be given by finding the eigen-value problem of the model. Assuming that the eigenvector of a translating system is $\Phi = [1 \;\; \phi_1 \;\; \phi_3 \;\; \phi_5]$, equation (9) holds from an eigen-value problem point of view. Solving equation (9) presents the modal mass $m_i^* = \Phi^t \mathbf{M}_p \Phi$.

$$\omega_{ni}^2 \mathbf{M}_p \Phi = \mathbf{K}_p \Phi, \quad i = 1,3,5 \tag{9}$$

Identify the natural frequencies ω_{ni} (where $i = 1,3,5$) from the open loop transfer function G_{op} shown in Figure 4(a) and make calculations to find the translating system's modal mass m_i^* as follows:

$$\{\omega_{n1}, \;\; \omega_{n3}, \;\; \omega_{n5}\} = \{21, \;\; 110, \;\; 312\} \quad \text{(Hz)}$$

$$\{m_1^*, \;\; m_3^*, \;\; m_5^*\} = \{71, \;\; 15, \;\; 21\} \quad \text{(kg)}$$

In the same fashion, derive the tilting system's modal mass from the natural frequencies ω_{ni} (where $i = 2,4,6$) of the open loop transfer function G_{ot} shown in Figure 4(b).

$$\{\omega_{n2}, \;\; \omega_{n4}\} = \{50, \;\; 80\} \quad \text{(Hz)}$$

$$\{m_2^*, \;\; m_4^*\} = \{16, \;\; 12\} \quad \text{(kg)}$$

- Step 3: Find a new open loop transfer function G_o^* from $H(s)$.

$$G_o^*(s) = \frac{G_r(s) + H(s)}{m^* s^2} \tag{10}$$

- Step 4: Define the sensitivity function of G_o^* as the Q-value function G_q.

$$G_q(s) \equiv \frac{1}{1 + G_o^*(s)} \approx \frac{s^2}{s^2 + 2\zeta\omega_n s + \omega_n^2} \approx \frac{1}{2\zeta} \tag{11}$$

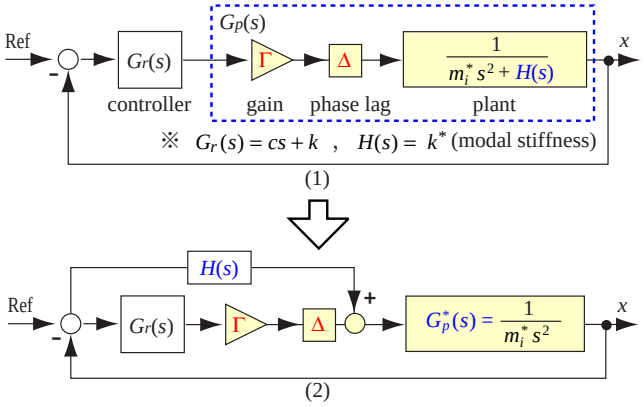

Fig. 6 Block diagram of AMB-rotor system

5-3. Evaluation of Q-value function

Table 1 and Figure 7 show the resulting Q-value function and the Q-value measured by the half power point. The former represents the Q-value as a peak amplitude at the critical speed N_{Ci} (where i = 1 to 5). Figure 7 says that the Q-value function provides almost the same results as the half power point. Accordingly, we believe that the proposed Q-value function is highly reliable and practical. Table 1 shows that the Q-value of the 3rd bending mode appearing at the critical speed N_{C5} has a maximum value of 13. From our experience, we are confident that balance corrections allow the rotor to pass N_{C5} if the Q-value does not exceed 20.

Table 1 Q-value

	N_{C1}	N_{C2}	N_{C3}	N_{C4}	N_{C5}
Peak of G_q	3.6	6.0	2.1	3.9	13
Half power	4.2	3.4	1.6	3.3	12

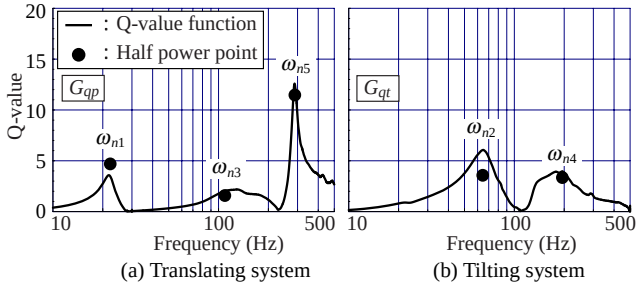

(a) Translating system (b) Tilting system

Fig. 7 Q-value function

6. ROTATIONAL TEST

6-1.Theory of Modal Balancing

High-frequency bending modes require precise balancing using a correction weight. In this study, we made balancing in the modal balancing method that uses eigen-modes based on the stiffness of an AMB [3]. Figure 8 shows eigen-modes actually measured when the AMB stiffness is about 1×10^6 N/m.

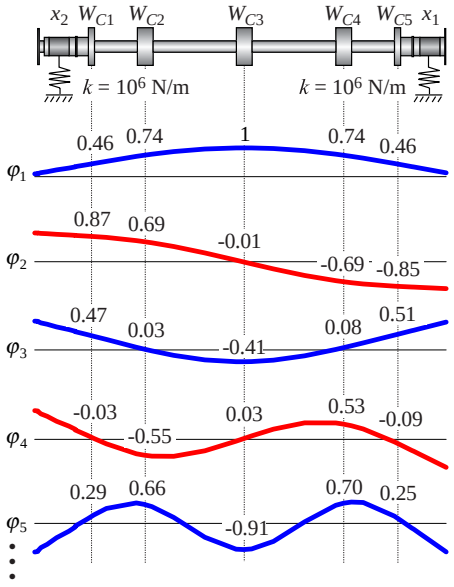

Fig. 8 Mode of the rotor (AMB stiffness = 1×10^6 N/m)

Converting the coordinates of equation (1) with the eigen-modes $\{\varphi_1, \varphi_2, \cdots, \varphi_5\}$ shown in Figure 8 presents a modal model represented by the following equation:

$$\mathbf{M}_\Psi \ddot{\boldsymbol{\eta}} + \mathbf{K}_\Psi \boldsymbol{\eta} = \left(\Psi^t \mathbf{U} + \Psi^t \mathbf{W}_c\right)\Omega^2 e^{j\Omega t} \tag{12}$$

$$\mathbf{X} = \begin{bmatrix}\varphi_1 & \varphi_2 & \cdots & \varphi_5\end{bmatrix}\begin{bmatrix}\eta_1 \\ \eta_2 \\ \vdots \\ \eta_5\end{bmatrix} = \boldsymbol{\Psi\eta}$$

where $\mathbf{M}_\Psi = \Psi^t\mathbf{M}\Psi$ is modal mass matrix, $\mathbf{K}_\Psi = \Psi^t\mathbf{K}\Psi$ is modal stiffness matrix, $\Psi^t\mathbf{U}$ is modal unbalance matrix, $\Psi^t\mathbf{W}_C$ is modal matrix representing the correction weight, Ω is rotational speed, and Ψ is mode conversion matrix.

In a modal model, each mode is represented as 1DOF system, which gives a mode-specific unbalance to each system. Accordingly, the weight ratio of a correction weight can be found so that it compensates for the unbalance indicated in the right side of equation (12), that is $\Psi^t\mathbf{U} + \Psi^t\mathbf{W}_C = 0$. For example, the weight ratio of mode φ_3 can be derived from the following equation that compensates for the unbalance at the mode φ_3 without affecting the modes φ_1 and φ_2 for which the balancing has already been made.

$$\begin{cases}\varphi_1^t\mathbf{W}_C = 0 \\ \varphi_2^t\mathbf{W}_C = 0 \\ \varphi_3^t\mathbf{W}_C = -\varphi_3^t\mathbf{U}\end{cases} \tag{13}$$

Solving equation (13) under $W_{C2} = W_{C4} = 0$ presents the weight ratio of correction weights. In the same fashion, the weight ratio of mode φ_4 can be derived from the modes $\varphi_1, \varphi_2, \varphi_3$ and φ_4, and $W_{C3} = 0$ as well as that of mode φ_5 from the modes $\varphi_1, \varphi_2, \cdots, \varphi_5$. Figure 9 shows these calculation results.

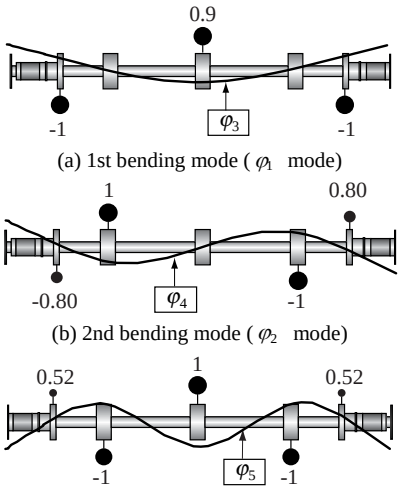

(a) 1st bending mode (φ_1 mode)

(b) 2nd bending mode (φ_2 mode)

(a) 3rd bending mode (φ_3 mode)

Fig. 9 Ratio of correction weight

6-2.Pass Test of Third Bending Critical Speed

Figure 10 shows the result of rotational test with the 2nd bending mode (φ_4 mode) balanced. We made balancing for the 1st and 2nd bending modes based on the mass ratios of correction weights shown in Figures 9(a) and 9(b). As shown in Figure 10, the vibration amplitude increased at 280 rps after the rotor passed the critical speed N_{C4} corresponding to the 2nd bending mode since the 3rd bending mode was unbalanced. Therefore, we made a decision that it was difficult to pass the critical speed N_{C5} = 295 rps corresponding to the 3rd bending mode, and made balancing for the 3rd bending mode at 280 rps. Placing a trial weight on each disk according to the mass ratio shown in Figure 9(c) changed the vibration amplitude at 280 rps from A to B as shown in Figure 10. The vector $\overrightarrow{AB}$ shows the effect of the trial weight. We made balancing by finding the weight and mounting angle so that the vector pointed to the origin of the polar plot.

Figure 12 shows the result of rotational test with the 3rd bending mode (φ_5 mode) balanced by the correction weight shown in Figure 11. It states that the vibration amplitude at 280 rps can be reduced from A to C. As a result, we have succeeded in enabling the rotor to pass the critical speed N_{C5} that corresponds to the 3rd bending mode.

Figure 13 shows a resonance curve resulting from the rotational test conducted after balancing. ISO 14839-2 defines the criteria for unbalance resonance amplitudes at the critical speed of an AMB-supported rotor. Zone A, the best performance, specifies 30 % of the AMB gap or less for the vibration amplitude.

If the resulting vibration amplitude is 150 μm_{p-p} or less, our rotor is ranked as Zone A. In this experiment, we were able to find the real eigen-modes from calculations under a boundary condition of 1×10^6 N/m and to make balancing through the modal balancing method in order to reduce the unbalance vibration amplitude to 150 μm_{p-p} or less (Zone A specified in the ISO standards) at all the critical speeds within a rated speed of 300 rps. As a result, the rotor reached 300 rps safely. Moreover, our method can cope with only the 3rd bending mode without affecting the other modes for which balancing has already been made.

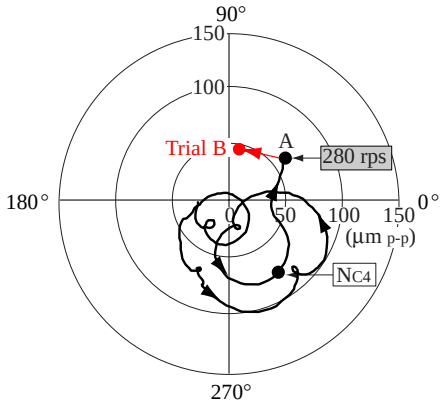

Fig. 10 Nyquist plot (passing the N_{C4})

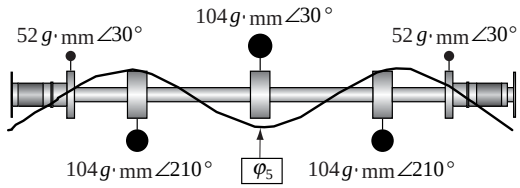

Fig. 11 Correction weight (5-plane balance)

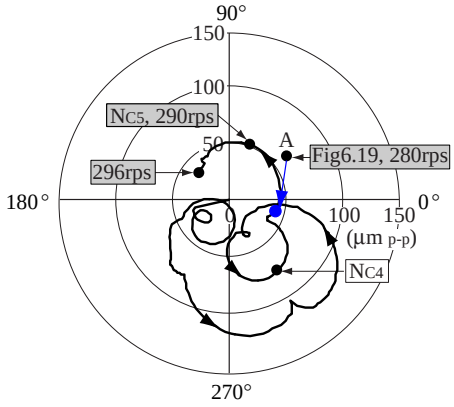

Fig. 12 Nyquist plot (passing the N_{C5})

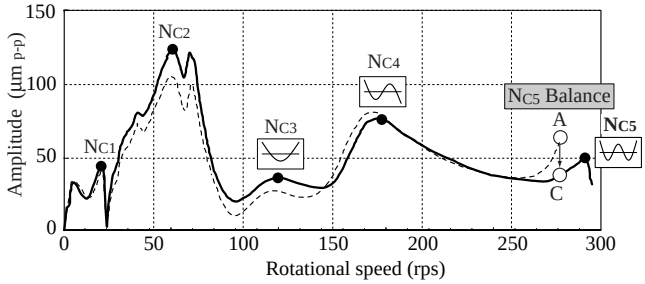

Fig. 13 Resonance curve

7. CONCLUSION

In this study, we have conducted elementary work to establish the technology of turning and controlling an AMB-supported symmetrical and flexible rotor so that it can safely pass high order bending critical speeds. Our conclusions are described below.

(1) We have proposed how to design a control system based on mode separation control method. Moreover, we have confirmed that our control system is effective through an evaluation of the stability margin based on the sensitivity function conforming to the ISO standards and of the damping performance according to the measured Q-value.

(2) We have proposed a new Q-value function for evaluating the Q-value in advance and confirmed its effectiveness through a comparison with measurement results given by the half power point.

(3) We have demonstrated that the modal balancing method is effective through a test in which the rotor passes the critical speed that corresponds to the 3rd bending mode, and succeeded for the first time in enabling an AMB-supported rotor to safely pass the 3rd bending critical speed N_{C5}.

We believe that our study not only presents important data for making rotors that are faster, longer, and lighter, but also contributes to the requirements for designing rotors incorporated into industrial AMB-supported rotating machines.

REFERENCES

[1] Y. Fukushima, et al, “Totally Oilless Centrifugal Compressor in Oil Refinery Service” Proc. of Advancements in Bearing and Seal Technology, 1994.

[2] R. Larsonneur, “Design and Control of Active Magnetic Bearing Systems for High Speed Rotation” Diss. ETH-Zurich Nr.9140, 1990.

[3] H. Fujiwara, et al, “Rotational Test of a Flexible Rotor Supported by Active Magnetic Bearings” Proc. of the 2nd Int. Symposium on Stability Control of Rotating Machinery, pp.188-198, 2003

[4] H. Fujiwara et al, “Control of Flexible Rotor Supported by Active Magnetic Bearings” Proc. of the ISMB-8, pp.145-150, 2002

[5] M. Ito, et al, “Evaluation of Stability Margin of Active Magnetic Bearing Control System Combined with Several Filters” Proc. of the ISMB-9, CD-ROM No.95, 2004

[6] O. Matsushita, et al, “Q-value Measurement for Damping Evaluation of AMB Rotor” Proc. of IEEE/ASME Int. Conf. on Advance Intelligent Mechtronics, pp.1083-1090, 2005.